中山大学 中山眼科中心 ZHONGSHAN OPHTHALMIC CENTER, SUN YAT-SEN UNIVERSITY

全文收录于 Lighthouse Scholar

眼科学报

官网：journal.gzzoc.org.cn



doi: 10.12419/25082801
View this article at: https://doi.org/10.12419/25082801

• 综 述 •

超声生物显微镜眼前段参数测量的标准化与规范化

陈立明 综述，肖 辉，叶一明，蔡小于，杨扬帆 审校

(中山大学中山眼科中心, 眼病防治全国重点实验室, 广东省眼科视觉科学重点实验室, 广州 510060)

文章亮点

1. 关键发现

• 超声生物显微镜 (ultrasound biomicroscope, UBM) 作为重要的眼前段影像检查设备，参数无统一标准，测量方法不规范，图像质量标准不足。加上操作干扰，声速设定偏差，影响参数测量的准确性，制约多中心研究。

• 本文提出了改进路径和规范化培训，明确参数定义及参数测量方法，建立分场景的图像质量标准，统一设备校准。

2. 已知和发现

• UBM 广泛应用于临床，操作者技术影响成像质量，UBM 与光学相干断层扫描 (opticalcoherence tomography, OCT) 测量存在差异，相关参数混乱但未系统梳理。

• 发现参数标准化缺失，发现测量方法不规范，发现图像质量标准不够详细，发现参数混乱的原因，并给出统一的建议。分场景化的图像质量标准确实导致误差增大。

3. 意义及改变

• 填补参数标准化空白，梳理规范测量方法，完善改进建议，提高数据可比性，为多中心精准研究提供帮助。

[摘　要]　超声生物显微镜 (ultrasound biomicroscope, UBM) 凭借高频超声 (50~100 MHz) 的特性突破了光学检查的局限，成为眼前段结构测量评估的重要工具，广泛应用于角膜病、青光眼、白内障、眼外伤、屈光手术等多个领域。但是，目前 UBM 参数测量仍然存在许多问题：参数标准化缺失导致同一参数的命名不同，或同一命名但定义不相同；测量方法不规范导致不同研究的对比性差；图像质量标准不够详细规范影响测量的准确性。这些问题影响了测量的精准性，也制约了多中心研究和数据互认。为此，本综述系统地梳理了角膜、前房、房角、虹膜、后房、晶状体及悬韧带、睫状体等 UBM 参数的标准测量方法，并归纳不同文献中的参数定义矛盾。分析测量误差的因素：声速设定与实际速度的偏差、接触式操作对眼球的干扰、操作者经验差异及与其他设备测量的客观差异等。在这个基础上，我们提出了改进方法：制定规范的检查流程、明确参数定义和测量方法、建立分场景图像质量标准及统一的设备校准方案。将来，UBM 参数测量将借助人工智能 (artificial intelligence, AI) 实现参数自动测量，结合三维成像技术、多普勒技术提升参数的全面性，向智能化和多维化发展，为眼科精准诊疗提供更全

收稿日期(Received): 2025-09-01; **修订日期(Revised):** 2025-09-24; **接收日期(Accepted):** 2025-10-30

通信作者(Corresponding author): 杨扬帆，Email: yangyangfan@gzzoc.com

作者贡献声明: 1) 构思设计：蔡小于；2) 行政支持：杨扬帆；3) 提供研究材料：肖辉，叶一明；4) 数据收集与汇总：陈立明，叶一明；5) 数据分析与解读：杨扬帆，陈立明；6) 稿件撰写：陈立明；7) 稿件最终修订与同意：所有作者

Contributions: Conception and design: CAI Xiaoyu; Administrative support:YANG Yangfan; Provision of study materials:XIAO Hui, YE Yiming; Collection and assembly of data: CHEN Liming, YE Yiming; Data analysis and interpretation: YANG Yangfan, CHEN Liming; Manuscript writing: CHEN Liming; Final approval of manuscript: All authors

电子全文

面的支持。
[关键词] 超声生物显微镜；眼前节；参数测量；标准化；人工智能
[中图分类号] R770.4 [文献标志码] A

引用本文: 陈立明, 肖辉, 叶一明, 蔡小于, 杨扬帆. 超声生物显微镜眼前段参数测量的标准化与规范化[J]. 眼科学报, 2026, 41(4): 313-324. DOI: 10.12419/25082801.

A review of the standardization and normalization of anterior segment parameter measurement using ultrasound biomicroscopy

CHEN Liming, XIAO Hui, YE Yiming, CAI Xiaoyu, YANG Yangfan

(State Key Laboratory of Ophthalmology, Zhongshan Ophthalmic Center, Sun Yat-sen University, Guangdong Provincial Key Laboratory of Ophthalmology and Visual Science, Guangzhou 510060, China)

Abstract The ultrasound biomicroscope (UBM), leveraging the characteristics of high-frequency ultrasound (50–100 MHz), has overcome the limitations of optical examinations and emerged as a crucial tool for measuring and evaluating anterior segment structures. It is widely applied in various fields, including corneal diseases, glaucoma, cataracts, ocular trauma, and refractive surgery. However, several issues persist in current UBM parameter measurements: the lack of parameter standardization results in different names for the same parameter or inconsistent definitions for parameters with the same name; non-standardized measurement methods lead to poor comparability across different studies; and inadequate and non-detailed image quality standards affect measurement accuracy. These problems undermine the precision of measurements and constrain multi-center research and data interoperability. To address these challenges, this review systematically outlines standardized measurement methods for UBM parameters related to the cornea, anterior chamber, anterior chamber angle, iris, posterior chamber, lens and zonular fibers, and ciliary body. It also summarizes contradictions in parameter definitions across different studies. Furthermore, factors contributing to measurement errors are analyzed, including discrepancies between the assumed and actual sound velocities, interference from contact-based operation on the eyeball, variations in operator experience, and objective differences compared to measurements from other devices. Building on this analysis, we propose improvement strategies, such as establishing standardized examination protocols, clarifying parameter definitions and measurement methods, developing scenario-specific image quality standards, and implementing unified device calibration schemes. In the future, UBM parameter measurement is expected to achieve automated parameter measurement with the aid of artificial intelligence (AI). By integrating three-dimensional imaging technology and Doppler techniques, it will enhance the comprehensiveness of parameters and evolve toward intelligence and multi-dimensionality, providing more holistic support for precision ophthalmic diagnosis and treatment.

Keywords ultrasound biomicroscope; anterior segment; parameter measurement; standardization; artificial intelligence

Cite this article as: CHEN Liming, XIAO Hui, YE Yiming, CAI Xiaoyu, YANG Yangfan. A review of the standardization and

normalization of anterior segment parameter measurement using ultrasound biomicroscopy[J]. Yan Ke Xue Bao, 2026, 41(4): 313-324. DOI: 10.12419/25082801.

眼前段结构的精准可视化与定量评估是眼科疾病诊断及治疗方案制定的重要环节。光学检查手段如房角镜、裂隙灯显微镜等，受限于穿透深度和分辨率限制，难以评估后房、晶状体悬韧带及睫状体等深层结构；光学相干断层扫描 (optical coherence tomography, OCT) 虽具备较高分辨率，但依赖透明光学介质，在角膜混浊、前房积血或致密组织遮挡时成像质量显著下降，形成临床诊疗中的“观察盲区”。20 世纪 90 年代初，超声生物显微镜 (ultrasound biomicroscope, UBM) 技术填补了这一空白[1]。该技术基于高频超声 (50~100 MHz)，通过不依赖光学介质的声波穿透特性实现了对眼前段深层结构的成像和测量。它还可以实时捕捉房角开闭动态、晶状体调节运动及睫状体位置变化，为生理解析和病理状态监测提供动态数据。

UBM 凭借高频超声的穿透特性和动态成像能力，已成为眼前段多维度评估的重要工具。有学者综述了其应用覆盖眼外肌异常、巩膜疾病、角膜病、青光眼、白内障、可植入式 Collamer 晶状体 (implantable contact lens, ICL) 手术、葡萄膜炎、眼外伤、眼部肿瘤及视网膜脱离等多个领域[2-3]。这些应用均离不开 UBM 对眼前段形态的精细观察和关键参数的量化分析。

但是，当前 UBM 参数体系面临着不少挑战：参数标准化缺失，同一参数存在多种命名或定义；测量方法不统一，同一参数在不同研究中的测量方法不一致；详细的图像质量标准尚未建立，跨研究数据可比性差。本文旨在系统梳理标准测量方法，并归纳不同文献中的参数定义矛盾，分析测量误差的因素，探索标准化改进路径与规范命名，为提升参数测量可靠性，推动多中心研究提供理论依据。

1　眼前段参数标准化测量方法

见图 1~9。

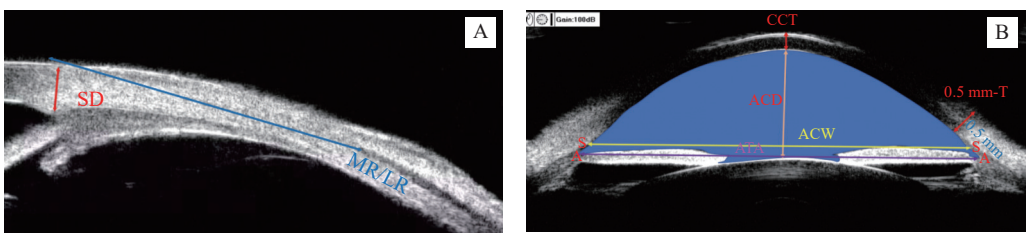


图 1　眼外肌、巩膜、角膜及前房参数测量示意图

Figure 1　Schematic diagram of parameter measurement for extraocular muscles, sclera, cornea and anterior chamber

巩膜厚度 (scleral thickness, SD)：巩膜突处巩膜外边界至内边界的距离[4]。眼外肌止端位置：角膜缘到眼外肌附着点的距离[5]。中央角膜厚度 (central corneal thickness, CCT)：中央角膜前表面到后表面的垂直距离[6]。巩膜突前 0.5 mm 处角膜厚度 (0.5 mm-thickness, 0.5 mm-T)[6]。中央前房深度 (anterior chamber depth, ACD)：中央角膜后表面到晶状体前表面的垂直距离[7]。房角顶点间距 (angle to angle, ATA)：双侧房角顶点之间的直线距离[8]。前房宽度 (anterior chamber width, ACW)：双侧巩膜突之间的直线距离[9]。前房面积 (anterior chamber area, ACA)：角膜内皮、房角、虹膜前表面和晶状体前表面包围的区域面积[10]。

Scleral Thickness (SD): The distance from the outer boundary to the inner boundary of the sclera at the scleral spur[4].Extraocular Muscle Insertion Position: The distance from the limbus to the attachment point of the extraocular muscle[5].Central Corneal Thickness (CCT): The vertical distance from the anterior surface to the posterior surface of the central cornea[6].0.5 mm Thickness (0.5 mm-T): The corneal thickness at the location 0.5 mm anterior to the scleral spur[6].Anterior Chamber Depth (ACD): The vertical distance from the posterior surface of the central cornea to the anterior surface of the lens[7].Angle to Angle (ATA): The straight-line distance between the apexes of the bilateral anterior chamber angles[8].Anterior Chamber Width (ACW): The straight-line distance between the bilateral scleral spurs[9].Anterior Chamber Area (ACA): The area enclosed by the corneal endothelium, anterior chamber angle, anterior surface of the iris, and anterior surface of the lens[10].

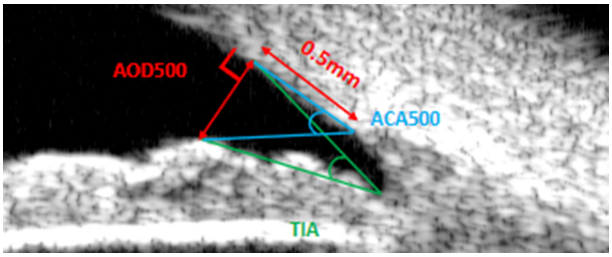


图 2 房角测量示意图 1

Figure 2 Schematic diagram 1 of anterior chamber angle measurement

0.5 mm 处房角开放距（angle opening distance at 500 μm, AOD500）：过巩膜突前 0.5 mm 小梁网处做垂线交于虹膜，该垂线的长度[4]。小梁-虹膜角：过巩膜突前 0.5 mm 小梁网处做垂线交于虹膜，房角隐窝顶点（trabecular-iris angle, TIA）[4]/巩膜突（anterior chamber angle 500 μm, ACA500）[9]与小梁网交点和虹膜交点形成的夹角。

Angle opening distance at 500 μm (AOD500): draw a perpendicular line through the trabecular meshwork 0.5 mm anterior to the scleral spur until it intersects the iris, and the length of this perpendicular line is the measured value[4]. Trabecular-iris angle: draw a perpendicular line through the trabecular meshwork 0.5 mm anterior to the scleral spur until it intersects the iris; this angle is formed by the intersection point of either the anterior chamber angle recess apex(trabecular-iris angle, TIA)[4]/the scleral spur (anterior chamber angle 500 μm, ACA500)[9] with the trabecular meshwork, and the intersection point of the aforementioned perpendicular line with the iris.

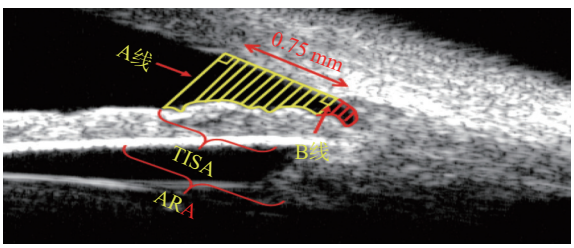


图 3 房角测量示意图 2

Figure 3 Schematic diagram 2 of anterior chamber angle measurement

角窝面积 (angle recess area at 750 μm, ARA750)：虹膜前表面、角膜内皮和 AB 线形成的三角形区域[11]。小梁-虹膜空间面积 (trabecular iris space area at 750 μm, TISA750)：虹膜前表面、角膜内皮、巩膜突处垂线和巩膜突前 0.75 mm 处垂线之间形成的封闭区域[11]。

Angle Recess Area at 750 μm (ARA750): The triangular area formed by the anterior surface of the iris, the corneal endothelium, and the AB line[11]. Trabecular Iris Space Area at 750 μm (TISA750): The enclosed area formed between the anterior surface of the iris, the corneal endothelium, the perpendicular line at the scleral spur, and the perpendicular line 0.75 mm anterior to the scleral spur[11].

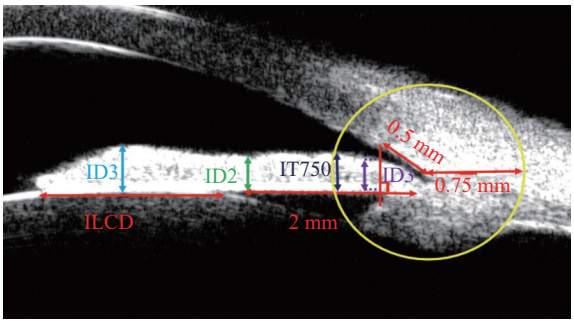


图 4 虹膜测量示意图 1

Figure 4 Schematic diagram of iris measurement 1

虹膜厚度 (iris thickness1/iris thickness2/iris thickness3, IT1/IT2/IT3)：距巩膜突前 0.5 mm 处作垂直虹膜的线，该线在虹膜上的长度/距离虹膜根部 2 mm 处的虹膜厚度/瞳孔缘处最大虹膜厚度[4]。虹膜厚度 (iris thickness at 750 μm from the scleral spur, IT750)：以巩膜突为圆心绘制半径 0.75 mm 圆，圆在虹膜前表面的交点到虹膜后表面的垂直距离[12]。虹膜-晶状体接触距离 (iris lens contact distance, ILCD)：虹膜与晶状体之间的距离[13]。

Iris Thickness1/Iris Thickness2/Iris Thickness3 (IT1/IT2/IT3): Draw a line perpendicular to the iris at the location 0.5 mm anterior to the scleral spur, where IT1 refers to the length of this line on the iris; IT2 is the iris thickness at the location 2 mm from the iris root; and IT3 is the maximum iris thickness at the pupillary margin[4]. Iris Thickness at 750 μm from the Scleral Spur (IT750): Draw a circle with a radius of 0.75 mm centered at the scleral spur, and the measured value is the perpendicular distance from the intersection point of the circle with the anterior iris surface to the posterior iris surface[12]. Iris Lens Contact Distance (ILCD): The distance between the iris and the lens[13].

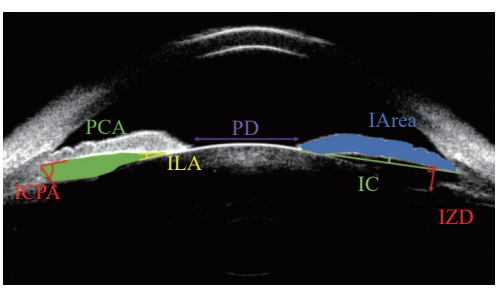


图 5 虹膜及后房测量示意图

Figure 5 Schematic diagram of iris and posterior chamber measurement

瞳孔直径 (pupillary diameter, PD)：双侧瞳孔缘之间的水平距离[9]。虹膜面积 (iris area, I-area)：整个虹膜长度的累积面积[14]。虹膜膨隆程度 (iris convexity, IC)：虹膜色素上皮

的起点与止点连线距离虹膜色素上皮层的最大垂直距离[15]。虹膜-晶状体角 (iris lens angle, ILA)：虹膜离开晶状体的角度[16]。虹膜-睫状体角 (iris-ciliary process angle, ICPA)：虹膜后表面与睫状体前表面的夹角[16]。后房面积 (posterior chamber area, PCA)：虹膜后表面、晶状体前囊膜、晶状体悬韧带及睫状体内表面围绕的面积[17]。晶状体悬韧带-虹膜距离 (lens zonule-iris distance, LZD)：睫状突悬韧带移行点处垂直虹膜的距离[18]。

Pupillary Diameter (PD): The horizontal distance between the bilateral pupillary margins[9]. Iris Area (I-area): The cumulative area of the entire iris[14]. Iris Convexity (IC): The maximum vertical distance from the line connecting the starting point and ending point of the iris pigment epithelium to the iris pigment epithelium layer[15]. Iris Lens Angle (ILA): The angle at which the iris detaches from the lens[16]. Iris-Ciliary Process Angle (ICPA): The angle between the posterior surface of the iris and the anterior surface of the ciliary body[16]. Posterior Chamber Area (PCA): The area surrounded by the posterior surface of the iris, the anterior capsule of the lens, the lens zonules, and the inner surface of the ciliary body[17]. Lens Zonule-Iris Distance (LZD): The distance perpendicular to the iris at the transition point of the ciliary process zonules[18].

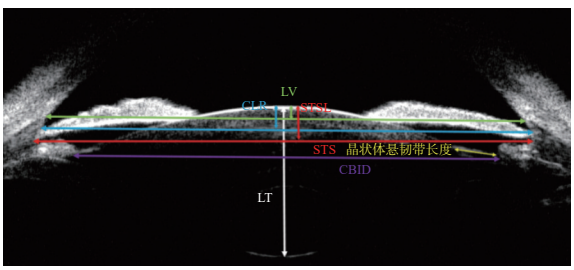


图 6　后房、晶状体及晶状体悬韧带测量示意图

Figure 6　Schematic diagram of posterior chamber, lens and zonule of zinn measurement

睫状沟间距 (sulcus to sulcus distance, STS)：双侧睫状沟之间的直线距离[19]。睫状体内径 (ciliary body inner diameter, CBID)：双侧睫状体最厚处的直线距离[20]。晶状体中心厚度 (Lens Thickness, LT)：晶状体中轴前囊膜到后囊膜的距离[21]。晶状体矢高 (crystalline lens raphe/lens vertex/sulcus-to-sulcus lens rise, CLR/LV/STSL)：双侧房角顶点连线[22]/巩膜突连线[23]/睫状沟连线[24]与中央部晶状体前囊膜的垂直距离。晶状体悬韧带长度：睫状突起点至前囊止点的长度[25]。

Sulcus to Sulcus Distance (STS): The straight-line distance between the bilateral ciliary sulci[19]. Ciliary Body Inner Diameter (CBID): The straight-line distance between the thickest parts of the bilateral ciliary bodies[20]. Lens Thickness (LT): The distance from the anterior capsule to the posterior capsule of the lens along its central axis[21]. Crystalline Lens Raphe/Lens Vertex/Sulcus-to-Sulcus Lens Rise (CLR/LV/STSL): The vertical distance between, respectively, the line connecting the bilateral anterior chamber angle apexes[22], the line connecting the bilateral scleral spurs[23], the line connecting the bilateral ciliary sulci[24], and the anterior capsule of the central part of the lens.Lens Zonule Length: The length from the starting point of the ciliary process to the ending point of the anterior capsule[25].

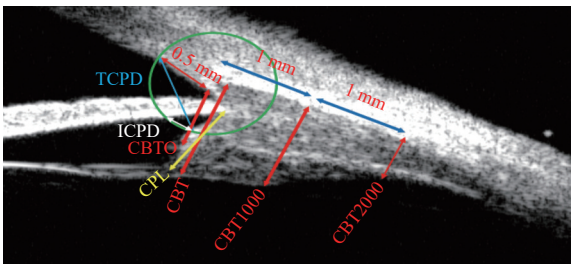


图 7　睫状体测量示意图 1

Figure 7　Schematic diagram of ciliary body measurement 1

睫状体厚度 (ciliary body thickness/ciliary body thickness at 0 μm/ciliary body thickness at 1 000 μm/ciliary body thickness at 2 000 μm, CBT/CBT0/CBT1000/CBT2000)：睫状体的最大厚度[26]/巩膜突处睫状体厚度[27]/巩膜突后 1 mm 处[28]/巩膜突后 2 mm 处[28]的睫状体厚度。睫状突长度 (ciliary process length, CPL)：虹膜睫状体交会处到睫状体内尖的距离[29]。小梁网-睫状体距离 (trabecular meshwork-ciliary process distance, TCPD)：He 法，以巩膜突为圆心，0.5 mm 为半径，交于小梁网及睫状体前表面，这两个交点的直线距离[12]。虹膜-睫状体距离 (iris-ciliary body distance, ICPD)：He 法，以巩膜突为圆心，0.5 mm 为半径，交于虹膜后表面及睫状体前表面，这两个交点的直线距离[12]。

Ciliary Body Thickness/Ciliary Body Thickness at 0 μm/Ciliary Body Thickness at 1 000 μm/Ciliary Body Thickness at 2 000 μm (CBT/CBT0/CBT1000/CBT2000): CBT refers to the maximum thickness of the ciliary body[26]; CBT0 is the thickness of the ciliary body at the scleral spur[27]; CBT1000 is the thickness of the ciliary body 1 mm posterior to the scleral spur[28]; and CBT2000 is the thickness of the ciliary body 2 mm posterior to the scleral spur[28]. Ciliary Process Length (CPL): The distance from the iris-ciliary body junction to the inner apex of the ciliary body[29]. Trabecular Meshwork-Ciliary Process Distance (TCPD): For the HE method, draw a circle with the scleral spur as the center and a radius of 0.5 mm, which intersects the trabecular meshwork and the anterior surface of the ciliary body; the measured value is the straight-line distance between these two intersection points[12]. Iris-Ciliary Body Distance (ICPD): For the HE method, draw a circle with the scleral spur as the center and a radius of 0.5 mm, which intersects the posterior surface of the iris and the anterior surface of the ciliary body; the measured value is the straight-line distance

between these two intersection points[12].

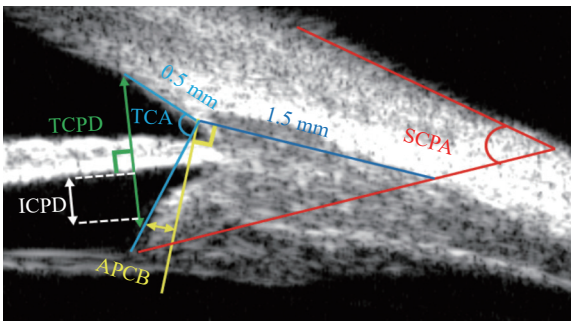


图 8 睫状体测量示意图 2

Figure 8 Schematic diagram of ciliary body measurement 2

小梁网-睫状体夹角 (trabecular meshwork-ciliary body angle，TCA)：以巩膜突为角，巩膜突与巩膜突前 0.5 mm 小梁网处连线作为一边，巩膜突与睫状体最前端连线为另一边[30]。小梁网-睫状体距离 (TCPD)：Pavlin 法，从巩膜突前 0.5 mm 的小梁网处作垂直虹膜后表面的线，止于睫状体，该线的长度[4]。虹膜-睫状体距离 (ICPD)：Pavlin 法，巩膜突前 0.5 mm 的小梁网处作垂直于虹膜的线交于虹膜后表面及睫状体前表面，这两个交点的直线距离[4]。睫状体前凸程度 (anterior protrusion degree of ciliary body, APCB)：巩膜突处作垂直巩膜内表面的线，睫状体前端到该线的垂直距离[29]。睫状体-巩膜夹角 (scleral-ciliary process angle, SCPA)：睫状体长轴与巩膜外表面的夹角[31]。

Trabecular Meshwork-Ciliary Body Angle (TCA): With the scleral spur as the vertex of the angle, one side is the line connecting the scleral spur to the trabecular meshwork 0.5 mm anterior to the scleral spur, and the other side is the line connecting the scleral spur to the anteriormost end of the ciliary body[30]. Trabecular Meshwork-Ciliary Process Distance (TCPD): For the Pavlin method, draw a line perpendicular to the posterior surface of the iris from the trabecular meshwork 0.5 mm anterior to the scleral spur, which extends to the ciliary body; the length of this line is the measured value[4]. Iris-Ciliary Body Distance (ICPD): For the Pavlin method, draw a line perpendicular to the iris from the trabecular meshwork 0.5 mm anterior to the scleral spur, which intersects the posterior surface of the iris and the anterior surface of the ciliary body; the measured value is the straight-line distance between these two intersection points[4]. Anterior Protrusion Degree of Ciliary Body (APCD): Draw a line perpendicular to the inner surface of the sclera at the scleral spur; the measured value is the vertical distance from the anterior end of the ciliary body to this line[29]. Scleral-Ciliary Process Angle (SCPA): The angle between the long axis of the ciliary body and the outer surface of the sclera[31].

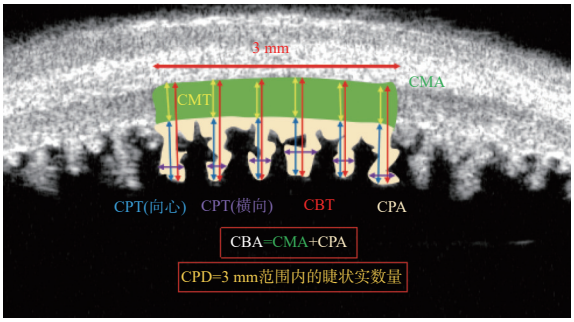


图 9 睫状体横截面测量示意图

Figure 9 Schematic diagram of ciliary body cross-sectional measurement

睫状体厚度 (CBT)：睫状突尖端到巩膜内表面的距离[32]。睫状肌厚度 (ciliary muscle thickness, CMT)：睫状突基底部到巩膜内表面的距离[32]。睫状突向心厚度 (ciliary process thickness, CPT)：睫状突尖端到睫状突基底部的距离[32]。睫状突环向厚度 (ciliary process circumferential thickness, CPT)：选择连续 5 个睫状突，测量其横向的最大距离，取平均值[33]。睫状突密度 (ciliary process density, CPD)：3 mm 范围内的睫状突数量[34]。睫状突面积 (ciliary process area, CPA)：3 mm 范围内所有睫状突的总面积[34]。睫状肌面积 (ciliary muscle area, CMA)：3 mm 范围内睫状肌总面积[34]。睫状体面积 (ciliary body area, CBA)：3 mm 范围内睫状体总面积[34]。

Ciliary Body Thickness (CBT): The distance from the tip of the ciliary process to the inner surface of the sclera[32]. Ciliary Muscle Thickness (CMT): The distance from the base of the ciliary process to the inner surface of the sclera[32]. Ciliary Process Thickness (CPT): The distance from the tip of the ciliary process to the base of the ciliary process[32]. Ciliary Process Circumferential Thickness (CPT): Select 5 consecutive ciliary processes, measure their maximum transverse distance, and take the average value[33]. Ciliary Process Density (CPD): The number of ciliary processes within a 3-millimeter range[34]. Ciliary Process Area (CPA): The total area of all ciliary processes within a 3-millimeter range[34]. Ciliary Muscle Area (CMA): The total area of the ciliary muscle within a 3-millimeter range[34]. Ciliary Body Area (CBA): The total area of the ciliary body within a 3-millimeter range[34].

2 参数测量的挑战与改进路径

2.1 技术局限性及操作挑战

声速设定偏差：UBM 默认使用 1 500 m/s 的基准速度与角膜真实传播速度 1 640 m/s 不符，导致测量误差。高频超声下多数眼组织真实传播速度仍不精确，这种理论假设与实际传播特性的偏

离直接影响测量精度[1]。

接触式干扰：UBM 的眼杯或探头压力可能改变眼球形态，可能影响参数测量的真实性[35]。在穿孔性眼外伤或角膜移植术后等特殊临床场景中，接触式操作不仅增加感染风险，还可能造成结构性损伤，导致 UBM 参数测量的应用受限[36]。

操作者依赖性：UBM 成像质量依赖操作者的经验。扫描切面的偏差，超声束与目标结构的非正交角度，眼球实时生理调节和眼球运动都是影响参数测量的重要因素。Gedde 等[37]认为需通过标准化培训降低人为误差。

与 OCT 参数测量的客观差异：Wan 等[35]发现 OCT 测量拱高为 (0.64±0.25)mm，显著大于 UBM (0.56±0.27)mm。他们之间的差异源于：1) 接触压力效应，可能会使眼前段形态改变；2) 调节反应差异，OCT 光源诱导瞳孔收缩和晶状体前移；3) 体位重力影响，OCT 检查时的坐姿晶状体更贴近日常状态，而 UBM 检查时仰卧位晶状体更贴近手术体位；4) 解剖标志识别，UBM 对睫状沟边界的超声反射信号更明确，OCT 易受虹膜色素干扰[3]。

2.2　参数体系的规范化困境

参数定义与测量标准的不统一严重制约 UBM 参数测量的广泛适用性和对比性，制约了 UBM 在多中心研究中的应用。例如，不同研究测量 CBT1 采用巩膜突后 1 mm[38]或 1.5 mm[39]作为测量起点，这种相同名称但定义不同使得对比时产生混乱。Pavlin[4]与 He[12]对于 TCPD 和 ICPD 的测量方法不同，但是其命名是一样的，同样容易产生混乱。未分场景的图像质量标准化进一步放大测量误差：目前放射状扫描以睫状突最大切面作为图像标准，但动态检查中最大的睫状突切面未必对应睫状突的解剖最前位点，导致 CBT、CBT1000 等反映睫状体厚度的参数与 TCA、TCPD 等反映前旋的参数存在客观矛盾和测量偏差；此外，STS 测量所需的充分暴露睫状沟切面，未必是睫状突最厚切面，造成 STS 与 CBID 之间的矛盾和测量偏差。见表 1 和表 2。

表 1　同一参数的不同缩写和使用建议

Table 1　Different abbreviations of the same parameter and their usage recommendations

参数	缩写	建议统一方案
房角开放度数	TIA[16]，θ1[4]	TIA
虹膜-晶状体夹角	ILA[40]，θ2[4]	ILA
虹膜-巩膜夹角	SIA[14]，θ3[4]	SIA
睫状体-巩膜夹角	SCPA[31]，θ4[4]	SCPA
巩膜突后1 mm/2 mm处睫状体厚度	CBT1000/CBT2000[41]，CBT1/CBT[28]	CBT＋距离
睫状突长度	CPD[42]，CPL[29]	CPL
睫状沟间距	STS[19]，SSD[43]，CSD[34]	STS
睫状体内径	CBID[44]，CRD[43]	CBID
睫状体厚度	CBT[26]，HCP[45]	CBT

表 2 同一缩写代表不同概念及使用建议

Table 2 Different concepts represented by the same abbreviation and their usage recommendations

缩写	测量方法	建议统一方案
ACA	定义1：前房角[43]；定义2：前房面积[10]	前房面积。表达前房角时：ACA+距离
PCA	定义1：后房角[45]；定义2：后房面积[19]	后房面积。表达后房角时：ICPA
CPL	定义1：虹膜睫状体交会处与睫状体内尖的距离[29]；定义2：睫状体内尖与巩膜突后1.5 mm处的距离[42]；定义3：睫状突水平方向的长度[20]	近年更多学者沿用定义1
CPD	定义1：睫状突长度[42]；定义2：睫状突密度[33]	睫状突密度
IT1000	定义1：距离虹膜根部1 mm处的厚度[9]；定义2：以巩膜突为圆心绘制半径1 mm的圆，交于虹膜前表面，交点垂直到虹膜后表面的距离[11]	近年更多学者沿用定义1
TCPD	定义1：从巩膜突前0.5 mm的小梁网处作垂直虹膜后表面的直线，止于睫状体，该线的长度[4]；定义2：以巩膜突为中心，半径0.5 mm作圆，交于小梁网和睫状突前表面，两个交点的距离[11]	近年更多学者沿用定义1
ICPD	定义1：从巩膜突前0.5 mm的小梁网处作垂直虹膜后表面的直线，交于虹膜后表面和睫状体前表面，两个交点的距离[4]；定义2：以巩膜突为中心，半径0.5 mm作圆，交于虹膜后表面和睫状突前表面，两个交点距离[11]	近年更多学者沿用定义1

2.3 改进方法

针对目前的困境，以下探讨提高利用 UBM 对眼前段参数测量准确性、重复性及可对比性的方法：

规范化培训：UBM 成像质量不仅依赖操作者的经验[37]，而且 UBM 的眼杯或探头压力可能影响眼球形态[35]，通过标准化培训可以降低人为误差。

明确参数定义：不同研究测量如巩膜突后睫状体厚度 (ciliary body thickness，CBT) 采用巩膜突后 1 mm 或 1.5 mm作为测量起点，这种 0.5 mm 的基准差异直接导致数据不可比性[46]。所以统一参数的命名及定义，规范参数测量方法，可以提高参数的可比性。

分场景化图像质量标准：针对不同参数的测量场景制定精细且可推广的图像质量标准，对于检查操作非常重要[47]，通过提高操作成像质量可以提高参数测量的精准性。

统一校准：虽然 OCT 与 UBM 测量拱高的差异源于接触压力效应、调节反应差异、体位重力影响和解剖标志识别[3]。但是设备之间的原理客观差异和校准差异值得纳入考量范围，通过建立不同设备间通用的校准工具及流程，对于控制不同设备的误差阈值有帮助。

3 未来展望

3.1 人工智能赋能 UBM 参数自动化测量

人工智能 (artificial intelligence, AI) 技术在医疗影像分析中的应用越来越广泛。基于深度学习的自动化模型能够提高测量的效率和保证测量准确性。多组织分割模型在自动识别前段结构和测量典型角度参数方面取得了显著成果，平均交并比 (intersection over union, IoU) 达到了 98%[48]。这都表明了 AI 技术在 UBM 图像测量分析中的巨大潜力。

3.2　三维成像技术与 UBM 参数测量

三维成像技术是 UBM 的另一项重要发展方向，补充现有 UBM 二维成像的不足。高分辨率三维超声成像技术对睫状体和虹膜后结构进行体内立体分析，可观察不同调节状态下的睫状肌变化[49]。未来，三维 UBM 技术有望与 AI 算法相结合，为临床提供更加全面和精准的眼前段参数测量方法。结合增强现实 (Augmented Reality,AR) 技术，三维 UBM 数据可实时叠加至手术视野，指导 ICL 襻定位、睫状体光凝等操作提供导航，提升手术精准度。

3.3　多普勒超声技术与 UBM 参数测量

多普勒超声技术已高度成熟，但其在 UBM 中的应用却鲜见报道。实际上，多普勒技术与 UBM 相结合对于眼前段血流参数测量评估具有重要价值，深化对疾病诊断机制的分析，潜在价值显著。

3.4　OCT 技术与 UBM 参数测量

UBM 在虹膜后结构成像上优于 OCT，而 OCT 在分辨率和图像边界清晰上更优，开发 UBM—OCT 同步扫描设备，依据不同的成像优势负责对应区域扫描，或分别扫描后依据不同区域的影像优势进行取舍，生成全景眼前节 UBM—OCT 图像，可构建更优的测量体系。

3.5　未来参数的研究重点

目前少有利用 UBM 测量参数来表达组织功能，功能化参数的开发具有积极意义，例如基于动态 UBM 成像开发虹膜弹性系数 (通过明暗光刺激下虹膜形态变化计算)、睫状体收缩速率 (单位时间内睫状突位移) 等功能指标，可能对揭示疾病早期的组织力学异常有帮助。

4　总结

本文综述了部分常用的眼前段参数，限于篇幅，并不全面；对于同一命名不同测量方法或者同一测量方法不同命名的情况也未完全覆盖；本文提出了分场景的图像质量标准化的重要性，但具体的实施步骤仍有待进一步研究和总结，此为本文尚待完善之处。

UBM 凭借高频超声波的穿透力和高分辨率优势，解决了虹膜后结构的可视化难题，为眼前段提供了不可替代的量化工具。其参数体系历经三十余年的发展，已经形成了系统的参数体系，推动眼科从“形态医学”向“形态医学＋量化医学”发展。但是，当前参数体系面临着多重挑战：参数标准化缺失，测量方法不统一，详细的图像质量标准尚未建立。未来需通过多级改进路径提高可靠性：制定规范的检查流程、明确参数定义和处理方法、建立分场景图像质量标准及统一的设备校准方案。UBM 的未来发展将以“标准化、智能化、功能化”为核心，通过 AI、三维技术、多普勒技术和 OCT 技术等突破操作瓶颈，拓展应用边界。虽然当前存在参数混乱与技术局限，但 UBM 在后房、晶状体悬韧带和睫状体的成像和参数测量仍然是不可替代的，是眼前段参数测量的重要工具。

声明

作者在研究和论文撰写中未使用生成式人工智能，所有作者对内容的真实性、完整性和科学性负责。所有科学贡献和智力劳动均由所有作者共同完成。

利益冲突　所有作者均声明不存在利益冲突。

开放获取声明

本文适用于知识共享许可协议 (Creative Commons)，允许第三方用户按照署名 (BY)-非商业性使用 (NC)-禁止演绎 (ND)(CC BY-NC-ND) 的方式共享，即允许第三方对本刊发表的文章进行复制、发行、展览、表演、放映、广播或通过信息网络向公众传播，但在这些过程中必须保留作者署名、仅限于非商业性目的、不得进行演绎创作。

参考文献

1. Pavlin CJ, Harasiewicz K, Sherar MD, et al. Clinical use of ultrasound biomicroscopy[J]. Ophthalmology, 1991, 98(3): 287-295. DOI: 10.1016/S0161-6420(91)32298-X.
2. 刘洋. 超声生物显微镜在眼科中的应用进展[J]. 世界最新医学

信息文摘, 2019, 19(93): 60-61. DOI: 10.19613/j.cnki.1671-3141.2019.93.029.

Liu Y. The applications and progression of ultrasound biomicroscopy in ophthalmology[J]. World Latest Med Inf, 2019, 19(93): 60-61. DOI: 10.19613/j.cnki.1671-3141.2019.93.029.

3. 常巍腾, 于志强. 有晶状体眼人工晶状体植入术后拱高的影响因素和测量技术[J]. 中国眼耳鼻喉科杂志, 2022, 22(5): 529-534. DOI: 10.14166/j.issn.1671-2420.2022.05.024.

Chang WT, Yu ZQ. Influencing factors and measuring techniques of vault after implantable collamer lens implantation[J]. Chin J Ophthalmol Otorhinolaryngol, 2022, 22(5): 529-534. DOI: 10.14166/j.issn.1671-2420.2022.05.024.

4. Pavlin CJ, Harasiewicz K, Foster FS. Ultrasound biomicroscopy of anterior segment structures in normal and glaucomatous eyes[J]. Am J Ophthalmol, 1992, 113(4): 381-389. DOI: 10.1016/S0002-9394(14)76159-8.

5. Duan R, Yang J. Comparison of anterior segment optical coherence tomography and ultrasound biomicroscopy in localizing horizontal rectus muscle insertions[J]. Eur J Ophthalmol, 2024, 34(3): 656-665. DOI: 10.1177/11206721231202539.

6. Drechsler J, Lee A, Maripudi S, et al. Corneal structural changes in congenital glaucoma[J]. Eye Contact Lens, 2022, 48(1): 27-32. DOI: 10.1097/ICL.0000000000000844.

7. Gao X, Zhou Y, Zuo C, et al. Predictive equation for angle opening distance at 750 μm after laser peripheral iridotomy in primary angle closure suspects[J]. Front Med, 2021, 8: 715747. DOI: 10.3389/fmed.2021.715747.

8. Li X, Chang P, Li Z, et al. Agreement between anterior segment parameters obtained by a new ultrasound biomicroscopy and a swept-source Fourier-domain anterior segment optical coherence tomography[J]. Expert Rev Med Devices, 2020, 17(12): 1333-1340. DOI: 10.1080/17434440.2020.1848541.

9. Xu Y, Tan Q, Li C, et al. The ocular biometry characteristics of young patients with primary angle-closure glaucoma[J]. BMC Ophthalmol, 2022, 22(1): 150. DOI: 10.1186/s12886-022-02374-2.

10. Wang D, Qi M, He M, et al. Ethnic difference of the anterior chamber area and volume and its association with angle width[J]. Invest Ophthalmol Vis Sci, 2012, 53(6): 3139. DOI: 10.1167/iovs.12-9776.

11. Bu Q, Hu D, Zhu H, et al. Swept-source optical coherencetomography and ultrasound biomicroscopy study of anteriorsegment parameters in primary angle-closure glaucoma[J]. Graefe's Arch Clin Exp Ophthalmol, 2023, 261(6): 1651-1658. DOI: 10.1007/s00417-022-05970-6.

12. He M, Friedman DS, Ge J, et al. Laser peripheral iridotomy in eyeswith narrow drainage angles: ultrasound biomicroscopyoutcomes. The Liwan Eye Study[J]. Ophthalmology, 2007, 114(8):1513-1519. DOI: 10.1016/j.ophtha.2006.11.032.

13. Yu Z, Wang X, Wang H, et al. Ultrasound biomicroscopic imaging analysis of lens position and stability in acute and chronic angle-closure glaucoma[J]. Front Ophthalmol, 2025, 5: 1624876. DOI: 10.3389/fopht.2025.1624876.

14. Zhou Y, Huang XB, Cai Q, et al. Comparative study of the effects of 1% atropine on the anterior segment[J]. J Ophthalmol, 2020, 2020: 5125243. DOI: 10.1155/2020/5125243.

15. Gong H, Dong X, Zheng B, et al. Ultrasound biomicroscopy might predict the outcome of phacoemulsification-visco dissection in medically controlled primary angle-closure glaucoma eye with extensive peripheral anterior synechia[J]. Front Med, 2021, 8: 705864. DOI: 10.3389/fmed.2021.705864.

16. Wang F, Wang D, Wang L. Exploring the occurrence mechanisms of acute primary angle closure by comparative analysis of ultrasound biomicroscopic data of the attack and fellow eyes[J]. Biomed Res Int, 2020, 2020: 8487907. DOI: 10.1155/2020/8487907.

17. 程天, 郭瑞萍, 郭安琪, 等. 超声乳化白内障摘除联合 IOL 植入术后眼前节结构变化及相关性分析[J]. 国际眼科杂志, 2024, 24(11): 1721-1727. DOI: 10.3980/j.issn.1672-5123.2024.11.06.

Cheng T, Guo RP, Guo AQ, et al. Structural changes in anterior segment after phacoemulsification combined with intraocular lens implantation and correlation analysis[J]. Int Eye Sci, 2024, 24(11): 1721-1727. DOI: 10.3980/j.issn.1672-5123.2024.11.06.

18. Zhang Z, Niu L, Liu T, et al. Primary observations of EVO ICL implantation for high myopia with concave iris[J]. Eye Vis, 2023, 10(1): 18. DOI: 10.1186/s40662-023-00335-4.

19. Tan W, Chen Q, Yang R, et al. Characteristics and factors associated with the position of the haptic after ICL V4C implantation[J]. J Cataract Refract Surg, 2023, 49(4): 416-422. DOI: 10.1097/j.jcrs.0000000000001134.

20. Xu Y, Liu F, Ye Y, et al. Establishment of a new vault prediction formula after implantable collamer lens implantation based on factor analysis of multi-modal ophthalmic parameters of anterior and posterior chamber[J]. Clin Exp Ophthalmol, 2024, 52(9): 920-933. DOI: 10.1111/ceo.14433.

21. Ríos-Elizondo CE, Bustamante-Vargas AP, Ramos-Betancourt N, et al. Ultrasound biomicroscopy insights: Ciliary body changes during accommodation in young adults[J]. Pan Am J Ophthalmol, 2025, 7(1): 137. DOI: 10.4103/pajo.pajo_14_25.
22. Baïkoff G, Bourgeon G, Jodai HJ, et al. Pigment dispersion and Artisan phakic intraocular lenses: crystalline lens rise as a safety criterion[J]. J Cataract Refract Surg, 2005, 31(4): 674-680. DOI: 10.1016/j.jcrs.2004.09.034.
23. Tang Y, Gao Y, Yu X, et al. Novel diagnostic indicators for acute angle closure secondary to lens subluxation based on anterior segment and lens parameters[J]. Heliyon, 2024, 10(3): e25164. DOI: 10.1016/j.heliyon.2024.e25164.
24. Wei R, Cheng M, Niu L, et al. Outcomes of the EVO ICL using a customized non-horizontal or horizontal implanting orientation based on UBM measurement: a pilot study[J]. Ophthalmol Ther, 2022, 11(3): 1187-1198. DOI: 10.1007/s40123-022-00498-8.
25. Gu X, Duan Q, He J, et al. Distribution and associations of anterior lens zonules lengths in patients with cataract[J]. Graefes Arch Clin Exp Ophthalmol, 2024, 262(8): 2515-2523. DOI: 10.1007/s00417-024-06379-z.
26. Mishima HK, Shoge K, Takamatsu M, et al. Ultrasound biomicroscopic study of ciliary body thickness after topical application of pharmacologic agents[J]. Am J Ophthalmol, 1996, 121(3): 319-321. DOI: 10.1016/s0002-9394(14)70282-x.
27. Wang Z, Huang J, Lin J, et al. Quantitative measurements of the ciliary body in eyes with malignant glaucoma after trabeculectomy using ultrasound biomicroscopy[J]. Ophthalmology, 2014, 121(4): 862-869. DOI: 10.1016/j.ophtha.2013.10.035.
28. Gohdo T, Tsumura T, Iijima H, et al. Ultrasound biomicroscopic study of ciliary body thickness in eyes with narrow angles[J]. Am J Ophthalmol, 2000, 129(3): 342-346. DOI: 10.1016/S0002-9394(99)00353-0.
29. Chen Q, Tan W, Lei X, et al. Clinical prediction of excessive vault after implantable collamer lens implantation using ciliary body morphology[J]. J Refract Surg, 2020, 36(6): 380-387. DOI: 10.3928/1081597X-20200513-02.
30. Chen SY, He N, Yan YJ, et al. Ultrasound biomicroscopic imaging demonstrate thinner ciliary body thickness in eyes with angle closure[J]. Int J Ophthalmol, 2022, 15(9): 1476-1482. DOI: 10.18240/ijo.2022.09.10.
31. Wenqing L I, Guizhen P A N, Ping S U N, et al. Characteristics of anterior segment structure in first-degree relatives of patients with primary angle-closure glaucoma[J]. International Eye Science, 2024: 111-116. DOI:10.3980/j.issn.1672-5123.2024.1.2.
32. Muftuoglu O, Hosal BM, Zilelioglu G. Ciliary body thickness in unilateral high axial myopia[J]. Eye, 2009, 23(5): 1176-1181. DOI: 10.1038/eye.2008.178.
33. Li J, Drechsler J, Lin A, et al. Repeatability and reliability of quantified ultrasound biomicroscopy image analysis of the ciliary body at the pars plicata[J]. Ultrasound Med Biol, 2021, 47(7): 1949-1956. DOI: 10.1016/j.ultrasmedbio.2021.03.002.
34. Ren J, Gao X, Chen L, et al. Characteristics of the ciliary body in healthy Chinese subjects evaluated by radial and transverse imaging of ultrasound biometric microscopy[J]. J Clin Med, 2022, 11(13): 3696. DOI: 10.3390/jcm11133696.
35. Wan T, Yin H, Yang Y, et al. Comparative study of anterior segment measurements using 3 different instruments in myopic patients after ICL implantation[J]. BMC Ophthalmol, 2019, 19(1): 182. DOI: 10.1186/s12886-019-1194-y.
36. Konstantopoulos A, Hossain P, Anderson DF. Recent advances in ophthalmic anterior segment imaging: a new era for ophthalmic diagnosis?[J]. Br J Ophthalmol, 2007, 91(4): 551-557. DOI: 10.1136/bjo.2006.103408.
37. Gedde SJ, Chen PP, Muir KW, et al. Primary angle-closure disease preferred practice pattern®[J]. Ophthalmology, 2021, 128(1): P30-P70. DOI: 10.1016/j.ophtha.2020.10.021.
38. Mohamed Farouk M, Naito T, Shinomiya K, et al. Observation of ciliary body changes during accommodation using anterior OCT[J]. J Med Invest, 2018, 65(1.2): 60-63. DOI: 10.2152/jmi.65.60.
39. Marchini G, Ghilotti G, Bonadimani M, et al. Effects of 0.005% latanoprost on ocular anterior structures and ciliary body thickness[J]. J Glaucoma, 2003, 12(4): 295-300. DOI: 10.1097/00061198-200308000-00002.
40. Yu Z, Wang F, Dong F, et al. Comparison of ocular morphological parameters related to lens position by anterior segment optical coherence tomography and ultrasound biomicroscopy[J]. Int J Clin Pract, 2022, 2022: 7599631. DOI: 10.1155/2022/7599631.
41. Ando T, Seki M, Ueda E, et al. A case of bilateral diffuse uveal melanocytic proliferation with secondary angle closure caused by ciliary body thickening[J]. Am J Ophthalmol Case Rep, 2022, 28: 101729. DOI: 10.1016/j.ajoc.2022.101729.
42. 马嘉, 陈晓明. 人眼睫状体在调节中形态与位置的动态变化[J]. 中华眼科杂志, 2004, 40(9): 590-596. DOI: 10.3760/j:issn:0412-4081.2004.09.005.

Ma J, Chen XM. Dynamic changes of configuration and position

of human ciliary body during accommodation[J]. Chin J Ophthalmol, 2004, 40(9): 590-596. DOI: 10.3760/j:issn:0412-4081.2004.09.005.

43. Marchini G, Pedrotti E, Modesti M, et al. Anterior segment changes during accommodation in eyes with a monofocal intraocular lens: high-frequency ultrasound study[J]. J Cataract Refract Surg, 2008, 34(6): 949-956. DOI: 10.1016/j.jcrs.2008.02.018.
44. Dougherty PJ, Rivera RP, Schneider D, et al. Improving accuracy of phakic intraocular lens sizing using high-frequency ultrasound biomicroscopy[J]. J Cataract Refract Surg, 2011, 37(1): 13-18. DOI: 10.1016/j.jcrs.2010.07.014.
45. Wu W, Liu J, Zhang L, et al. Development and validation of a novel vault prediction formula based on structural parameters of the anterior and posterior chambers[J]. BMC Ophthalmol, 2024, 24(1): 349. DOI: 10.1186/s12886-024-03609-0.
46. Warjri GB, Senthil S. Imaging of the ciliary body: a major review[J]. Semin Ophthalmol, 2022, 37(6): 711-723. DOI: 10.1080/08820538.2022.2085515.
47. 陈立明, 杨扬帆, 李轶擎. 实用眼科超声生物显微镜图谱[M]. 广州: 广东科技出版社, 2025: 266-278.
Chen LM, Yang YF, Li YQ. Practical atlas of ophthalmic ultrasound biomicroscopy[M]. Guangzhou: Guangdong Science & Technology Press, 2025: 266-278.
48. Li F, Zhang X, Yang K, et al. Deep learning-based anterior segment identification and parameter assessment of primary angle closure disease in ultrasound biomicroscopy images[J]. BMJ Open Ophthalmol, 2025, 10(1): e001600. DOI: 10.1136/bmjophth-2023-001600.
49. Stachs O, Martin H, Kirchhoff A, et al. Monitoring accommodative ciliary muscle function using three-dimensional ultrasound[J]. Graefes Arch Clin Exp Ophthalmol, 2002, 240(11): 906-912. DOI: 10.1007/s00417-002-0551-2.

(责任编委: 陈子东; 编辑: 殷秋霞)